Penerbit Akademia Baru

Journal of Advanced Research in Experimental Fluid Mechanics and Heat Transfer

Journal homepage: http://www.akademiabaru.com/submit/index.php/arefmht
ISSN: 2756-8202

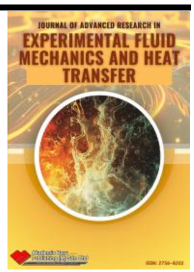

Enhanced Aerodynamic Performance of NACA 0009 Morphing Airfoil: A Study on Camber Morphing and Vortex Generators

Sharul Sham Dol[1,*], Joaquin Rafael Pagaling[1], Dana Almansoori[1], Hasan Hamdan[1], Kamarul Arifin Ahmad[2]

[1] Department of Mechanical Engineering, Faculty of Engineering, Abu Dhabi University, Abu Dhabi, United Arab Emirates
[2] Department of Aerospace Engineering, Faculty of Engineering, Universiti Putra Malaysia 4300 Serdang, Selangor, Malaysia

ARTICLE INFO

Article history:
Received 12 March 2025
Received in revised form 10 April 2025
Accepted 5 may 2025
Available online 30 June 2025

Keywords:
Biomimicry; aerodynamics; turbulent kinetic energy; turbulent intensity; lift; drag; vortex generators; flow separation; camber; morphing; Q-criterion

ABSTRACT

This study investigates the aerodynamic benefits of adaptive morphing airfoil that include camber morphing with vortex generators, focusing on their impacts on lift, drag and flow management. It involves CFD simulations of a NACA 0009 airfoil were performed on four methods: uncambered without vortex generators, uncambered with vortex generators, cambered without vortex generators and cambered with vortex generators; additionally, these simulations analysed lift-to-drag ratios, boundary layer stability and flow separation across a range of angles of attack (AOA). The results clearly demonstrate the good performance of the cambered airfoil with vortex generators, which had the highest lift-to-drag ratio, delayed flow separation and greatly improved boundary layer stability, particularly at higher angles of attack. Furthermore, the CFD simulations were highly supported by the flow visualization results, which demonstrated a strong link between wake generation, flow separation patterns and pressure distribution. At increasing angles of attack, the observed start of stall and wake turbulence closely matched the simulation findings, confirming the accuracy of the results. Nonetheless, camber morphing improved flow circulation around the airfoil, resulting in more lift generation, while vortex generators stimulated the boundary layer, thereby delaying separation and decreasing drag. This study underlines the significance of combining camber morphing and vortex generators into airfoil designs, offering a transformative approach to addressing critical issues in modern aviation, such as fuel efficiency and operational flexibility; finally, the findings provide a solid platform for future developments in morphing airfoil technology and its practical application in aerospace engineering.

1. Introduction

The concept of aircraft morphing leads to significant advances in aerodynamic performance and flight control. Simply put, morphing wings alter the geometry or shape of a wing; these wings are constructed using a variety of morphing procedures aimed at improving aircraft performance and stability [1,2]. Morphing wings are gaining popularity in the aviation sector because of their ability to

* *Corresponding author.*
E-mail address: sharulshambin.dol@adu.ac.ae (Sharul Sham Dol)

https://doi.org/10.37934/arefmht.20.1.4167

improve agility and fuel efficiency. Morphing wings, unlike traditional wings with a fixed shape, can change their arrangement due to their transforming nature [3]. Furthermore, for optimal low-speed performance, an aircraft's wings must have a high aspect ratio and a low sweep angle, whereas a low aspect ratio and a high sweep angle are ideal for high-speed flights [4-6]. A morphing wing may adapt to various configurations, lowering drag and boosting aerodynamic performance. Furthermore, this adaptability results in increased fuel efficiency and better flexibility in aircraft design and operation. In addition, the National Aeronautics and Space Administration (NASA) and the Massachusetts Institute of Technology (MIT) have created morphing wings, which have been tested in the aviation sector [4-6]; research on these unique wings is on development and it has been shown that morphing wings have large potential to enhance aircraft production, flight and maintenance efficiency [7]. Moreover, the morphing wing concept has evolved over time to improve the aerodynamic performance of aircraft; it is divided into two categories: airfoil-level morphing and wing-level morphing [8]. These notions have already been used, tested and studied over time and this aircraft technology enhance lift and drag coefficients, flight control and other aerodynamic characteristics [9].

1.1 Literature Review

Succeeding the previous research on Avian-inspired morphing trailing-edge flaps, Akhter *et al.,* [9] developed a bionic morphing flap to mimic feather movements, morph spanwise and vary its camber to generate seamless wave-like formations at the trailing-edge. Based on the S809 airfoil with chord length = 0.443 m and span of 1 m, opted due to its well-known prominence and robust airfoil characteristics, the bionic morphing flap aimed to achieve optimal aerodynamic performance, such as enhanced glide ratio, drag reduction and lift enhancement. In addition, conducted at free stream velocity of U = 33 m/s which correlates to a low Reynolds number of 10^6, CFD simulations were conducted to gain valuable insights into the airfoil’s flow field characteristics and boundary layer dynamics in the vicinity of morphing trailing-edge at varying deformation angles and angles of attack. Unsteady Reynolds-Averaged Navier Stokes equations (URANS), 2-equation eddy-viscosity k-omega SST model are the respective governing equations and turbulence modelling used [9]. Results revealed the pressure coefficient Cp gradient, in the midplane and quarter planes area of the morphing wings, amplified with increase in flap deflection angle and angle of attack. Furthermore, in contrast to conventional flaps, the morphing flaps have lower Cp in the lower leading-edge suctional peak, the point of lowest pressure of the airfoil, but adverse the pressure build-up once $\beta = 15°$ and $\alpha = 0°$, leading to early flow separation, leading to minimized lift and increases pressure drag around the leading-edge, as demonstrated by Figure 1 [10].

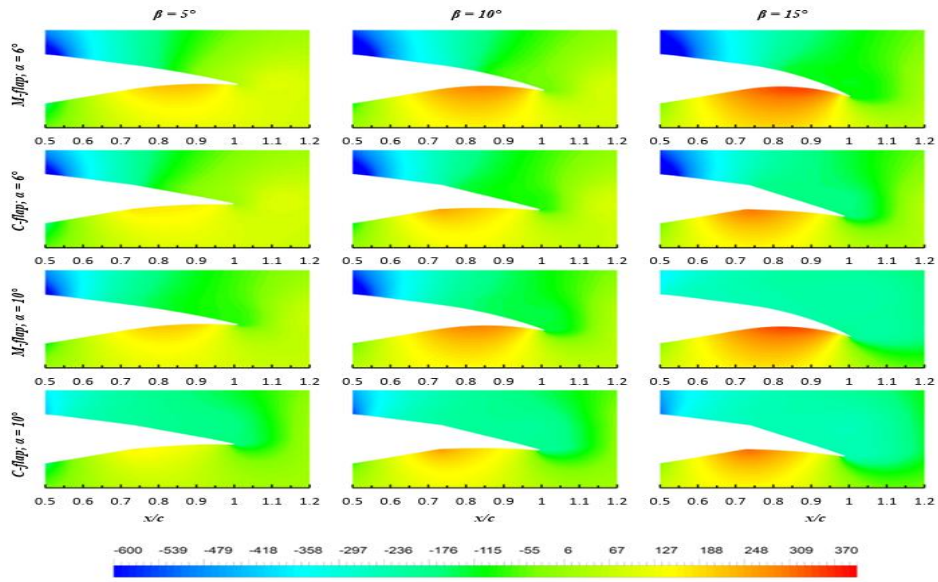

Fig. 1. Pronounced variance in pressure drag [10]

Varying the wing camber provides more controllability to the aerial vehicle's lift, stability and versatility which depends on their implementation, shown by Figure 2 [11]. The wing's morphing leading and trailing edges can have differential camber variation which leads to many benefits. For instance, Jawahar *et al.,* [12] pinpointed a morphing leading-edge reduces airframe noise and promote laminar flow, thereby reducing induced drag, whereas a morphing trailing-edge generates smooth contours with tight tolerances. Jawahar *et al.,* [12] performed experimental and numerical investigations of a NACA 0012 airfoil, chosen due to its aerodynamic characteristics that allowed varying camber profile treated as morphing trailing edges to occur throughout the trials. The specimen was then tested with flaps with varying camber profile for deflection angles $\beta = 5°$ and $\beta = 10°$ and angles of attack ranging from $\alpha = -5°$ to $20°$. Results revealed changes in lift coefficient are influenced by the morphing trailing-edge's size, curvature and deflection angle. In terms of pressure distribution, at low angles of attack, a noticeable distinction was observed between the hinged flap and morphing flap airfoil; the hinged flap achieved roughly 40 % lower C_P suction peak close to the leading-edge [13]. Such difference subsided once the AOA increased gradually. In terms of wake flow development, the onset of flow separation was further noticed in the morphing airfoil further far-wake downstream locations at higher AOA than that of hinged flaps [12].

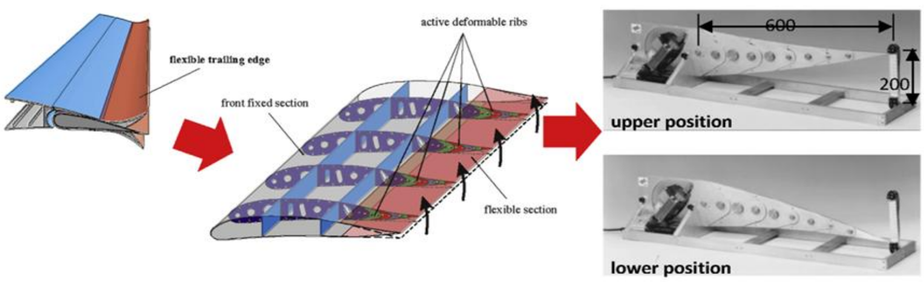

Fig. 2. Actuation mechanism of camber morphing [11]

The non-dimensional turbulent kinetic energy (TKE) calculated by hotwire tests revealed larger magnitudes for morphing airfoil in the wake region toward the pressure side, which peaked at x/c = 2.015 [12]. The iso-surfaces of the Q-criterion shown by Figure 3 shows a more significant wake velocity deficit for morphing airfoil between x/c = 0.8 and x/c = 0.95 than the hinged airfoil, which accounts for larger TKE and wider wake region development [14]. In terms of the non-dimensional boundary layers, the hinged airfoil experienced early boundary separation which led to recirculation region and vortices that led to substantial loss of energy, whereas the morphing airfoil displayed later boundary separation due to its smoother flap curvature, thereby increasing velocity and reduced pressure near the suction sides [13,14]. In addition, it exhibited thicker boundary layers which verified results of the Q-criterion; the reason behind such exhibited behaviours was the higher shear stress and velocity in the suction side experienced by the morphing airfoil, which further delayed the onset of flow separation at the further downstream location x/c = 0.90. At $\alpha = 4°$, both for the hinged and morphing airfoils were localized on the suction side of the flap revealed by Figure 3, but flow separation was more delayed for morphing airfoil due to thicker high-intensity region that initiated downstream at x/c = 0.90 [15].

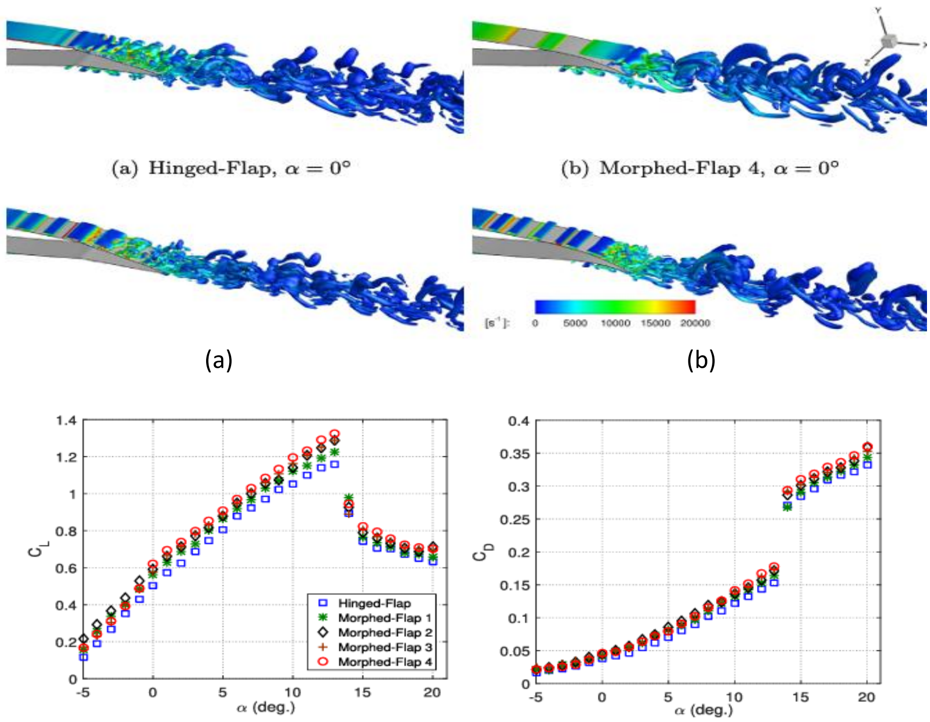

(c)

Fig. 3. (a) Cl and Cd increases linearly until AOA = 15 degrees (b) Hinged flap (c) Morphing flap flow separation [11]

Table 1 summarizes both applications in structural and aerodynamic analysis of the theory of morphing wings included various configurations, such as variable camber, variable sweep and twisting morphing. Li *et al.,* [1] noted 2D morphing concepts were simpler to create and provide higher fidelity compared to 3D concepts, so parameters that were best studied within the 2D domain are airfoil parameters - variable camber and variable thickness, whereas wing-level morphing actions like span and twist morphing and wing folding mechanisms were limited within the 3D domain [1].

Table 1
Morphing methods with distinct characteristics

Morphing Strategy	Purpose	Morphing Level
Variable Camber	Performance Cl/Cd	
	Noise Reduction	Low
	Flight Control (roll, pitch, yaw)	
Variable Thickness	Performance Cl/Cd	
	Low-speed performance improvement	Low
Twist Morphing	Flight Control (roll, pitch, yaw)	Medium
Span Morphing	Performance Cl/Cd	High
	Flight Control (roll)	
Variable Sweep	Performance Cl/Cd	
	Flight Control (Turn Radius)	High
	Disturbance rejection (crosswind)	
Folding wing	Performance Cl/Cd	High

Flow-separation control can improve existing fluid-dynamical systems and aid in conceptual design from the start of the product development process [16,17]. In fluid dynamics, "flow separation control" refers to modifying a wall-bounded fluid flow via devices such as vortex generators or simply VGs [18,19]; the fundamental benefit of using VGs in wall bounded flows is that they can delay and/or avoid boundary-layer separation, which increases overall system efficiency [19]. For example. airfoils modified with added winglets at blade tips to eliminate the trailing vortices strength [20]. When running beyond their operational envelope, fluid-dynamic systems may require flow separation control. Knepper [21] investigates the usage of trailing-edge serrated vortex generators to improve aerodynamic performance. Vortex generators are meant to activate the boundary layer, delaying flow separation, which is vital during the take-off and landing phases when lift is critical; by energizing the boundary layer and delaying flow separation, these devices improve lift and control, especially during take-off and landing demonstrated by Figure 4 [17,22]. Furthermore, triangular serrations, when properly positioned, create vortices that increase boundary layer momentum, keeping it linked to the wing surface for longer and improving lift generation and flight characteristics. To validate the results, CFD analysis was integrated with wind tunnel testing. The study found a positive correlation between computational and experimental data, indicating that serrations influence flow patterns and reduce early separation, particularly at higher angles of attack [18,22]. The study also discovered that bigger deflection angles of serrations produced stronger vortices, but they decayed faster than smaller angles, stressing the need of optimizing serration design for maximum effectiveness [23].

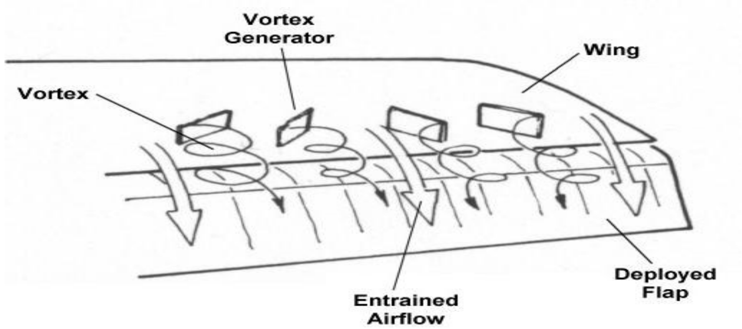

Fig. 4. Vortex generator working principle [22]

Therefore, the primary objective of this study is to evaluate the aerodynamic performance of an adaptive morphing airfoil, based on a NACA 0009 airfoil, using CFD simulations. This study also intends to quantify the impacts of camber morphing and flow control devices on aerodynamic efficiency by comparing four different cases: uncambered with and without vortex generators and cambered with and without vortex generators. Furthermore, it focuses on critical factors such as lift coefficient Cl, drag coefficient Cd, lift-drag coefficient ratio Cl/Cd and flow separation characteristics at different angles of attack. CFD is used to provide high-resolution insights into flow phenomena, allowing for thorough comparisons of the airfoil's performance increases in each configuration.

2. Methodology

2.1 Design and CFD Setup

Table 2 reveals the required steps to be taken to design an adaptive morphing airfoil.

Table 2
Steps to take for importing design

Step	Task	Software Approach	Works Done
1	Create 3D geometry using Fusion 360	Fusion 360	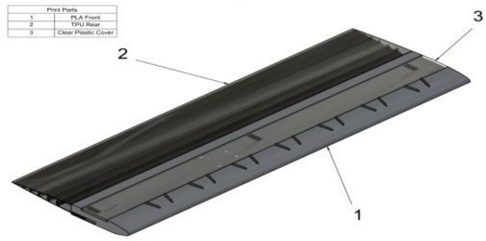
2	Importing 3D geometry and creating domain in Design Modeler	ANSYS Design Modeler	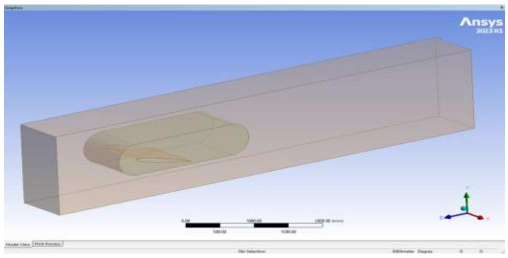 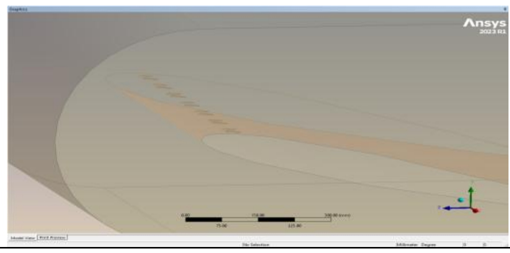

For accurate and precise results, the linear tetrahedral elements are employed to generate the mesh for the model, shown in Figure 5. It has 4 nodes per element and approximately 900,500 elements.

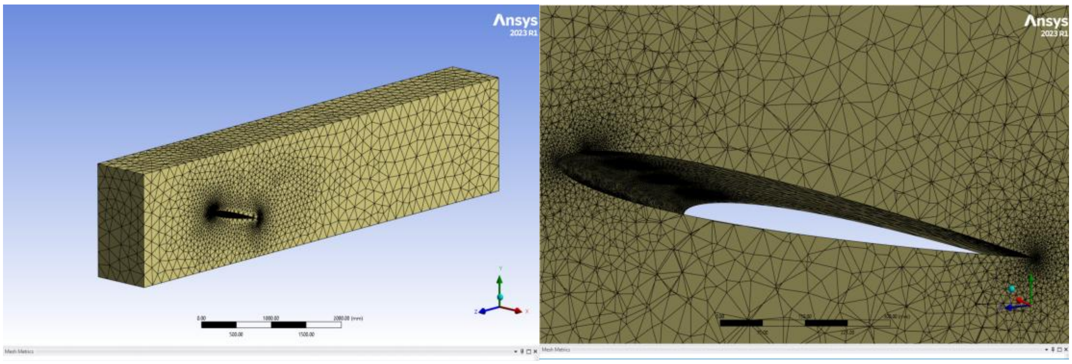

Fig. 5. Concentrated meshing near sharp curvatures

Table 3 tabulates the key parameters and user – defined values. Furthermore, to refine the mesh quality around the sharp edges, such as the vortex generators, edge sizing was the most appropriate to be used. Bias Factor of 150 and near to the vortex generators' surfaces were decided for capturing their fine details in the simulation.

Table 3
Meshing parameters

Parameter	Value
Element Size (mm)	30
Growth Rate	1.15
Max Element Size (mm)	50
Mesh Defeaturing	Yes
Defeaturing Size (mm)	2.5e-4
Curvature Min. Size (mm)	1.2
Curvature Normal Angle (°)	16.5
Capture Proximity	No
Check Mesh Quality	Yes, Some Errors
Smoothing	Medium
Mesh Metric	Skewness
Maximum Layers of Inflation	5
Growth Rate of Inflation	1.15

Next, Table 4 tabulates the simulation parameters and controlled values. Based on the literature papers reviewed, a Reynolds number of approximately 970,000 is the optimal value, which translates that the morphing airfoil reaches a turbulent regime. Furthermore, it is a justifiable number in low-to-moderate speed applications, such as small UAVs or controlled wind tunnel testing, making it appropriate for evaluating the aerodynamic performance of the morphing airfoil without approaching high-speed or transonic regimes that require more complex models. Also, boundary layer effects and flow separation at this velocity, particularly at the trailing edge and vortex generators, provide a clear understanding of how the morphing process impacts lift, drag and flow control. Moreover, this Reynolds number maintains processing efficiency by eliminating the requirement for highly refined meshes, which is necessary at higher velocities. Most importantly, a range of Angle of Attack (AOA) is tested to determine not only the relationship between coefficient of lift and drag but also investigate the airfoil's critical angle of attack and analyse any trend as a consequence of increasing AOA. k-ω SST turbulence model was used since it is well-suited for our techno-economic analysis; that is, it is a robust, reliable model for capturing surface boundary layer. In addition, it is quite effective and efficient in handling adverse pressure gradients, especially at high AOAs. Compared to other models like LES, the k- ω SST has the balance of good accuracy whilst being computationally friendly.

Table 4
Simulation parameters

Parameter	Value
Solver Type	Pressure – Based
Time	Transient
Gravity (m/s^2)	-9.81 in Y - axis
Turbulence Model	k – omega (2 eqn)
k – omega model	SST
Angle of attack (α in °)	0-25 (Range)
Inlet Boundary Condition Speed (m/s)	44.32
Outlet Gauge Pressure (Pa)	0
Outlet Backflow Turbulent Intensity (%)	3.5
Backflow Turbulent Viscosity Ratio	7
No – Slip Treatment	Yes
Symm	N/A
Operating Pressure (Pa)	101325
Operating density (kg/m^3)	1.225
Solution Method	COUPLE with 2nd order Spatial Discretization
Report Definitions	Cl, Cd
Initialization Type	Hybrid
Number of Time Steps	5000
Time Step Size (s)	0.01
Max Iterations/Time Step	200
Reporting Interval	10
Profile Update Interval	10

2.2 Experimental Setup

To validate our CFD findings, we conducted wind tunnel experiments, visualized by Figure 6, using a carefully controlled setup designed to visualize airflow behaviour around the airfoil. First, the airflow was initiated through a smoothly contoured intake, ensuring minimal disturbances as it entered the test section, where the airfoil was securely mounted using adhesives to prevent unwanted vibrations or misalignment.

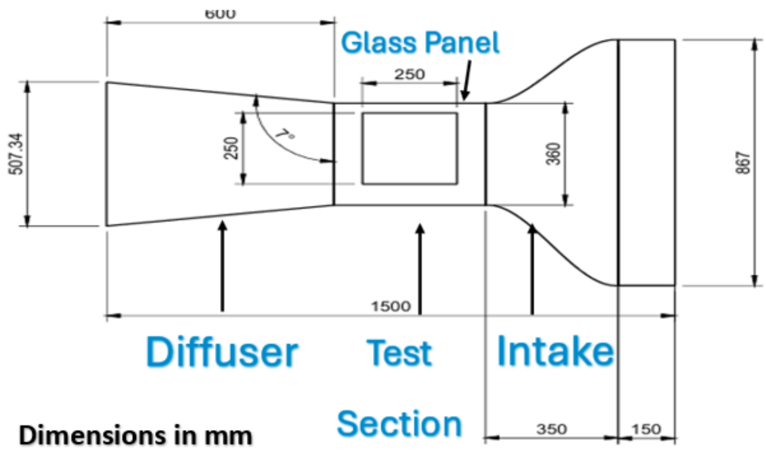

Fig. 6. Wind tunnel schematic. Airflow moves from right to left

Furthermore, a fan shown at Figure 7, positioned at the diffuser, created a suction-driven flow, pulling air smoothly through the system and maintaining a steady freestream velocity.

Fig. 7. Fan mounted at the diffuser section

The most critical aspect of this setup is to promote laminar flow early in the intake section, so honeycomb meshes, demonstrated by Figure 8, were installed both upstream and downstream of the test section. These straightened the airflow, promoting laminar entry conditions and minimizing turbulent fluctuations at the exit.

Fig. 8. 3D printed honeycomb mesh

Furthermore, for flow visualization, a smoke generator produced a continuous stream of tracer particles, which were carefully injected into the airstream using a smoke rake positioned upstream of the airfoil. The rake ensured uniform smoke injection, enabling clear observation of streamline attachment, flow separation and wake development shown in Figure 9. Then, as air exited through the diffuser, it expanded gradually, reducing flow disturbances that could affect visualization quality.

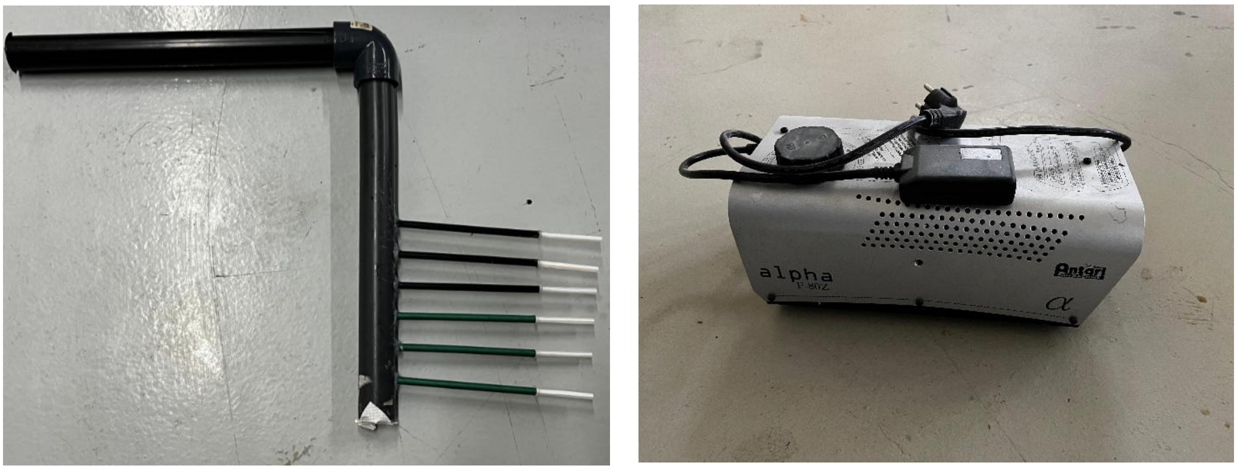

(a) (b)

Fig. 9. (a) Smoke rake with straws attached (b) Smoke generator

In addition, using a sturdy camera mount, a high-quality camera was positioned to record high-resolution video and photos of the airflow behaviour to improve data collecting and visualization. LED lighting was also placed throughout the test area to provide the best possible lighting, lowering shadows and boosting smoke contrast for improved visibility. Most importantly, the test section is fully covered in black, except the viewing panel, so no external light goes through it as shown by Figure 10.

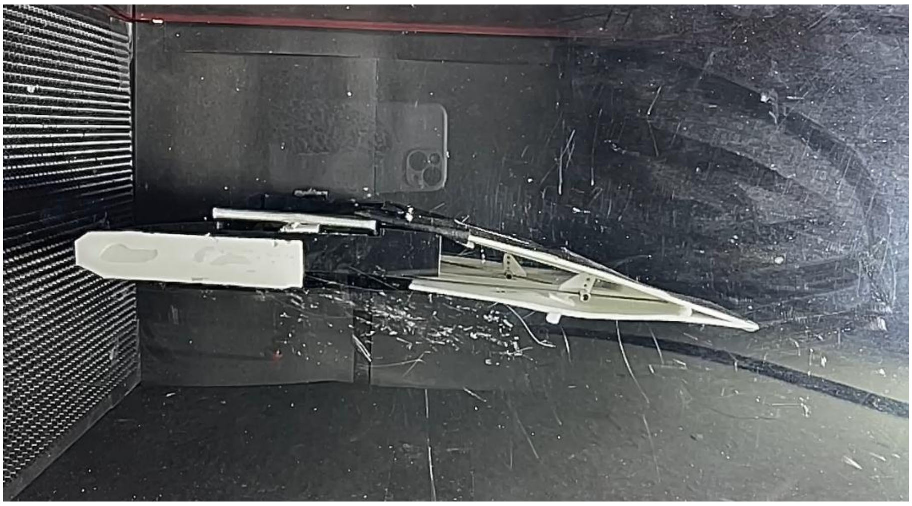

Fig. 10. Setup in the test section. Camera with camera mount reflecting off viewing panel. Airfoil mounted using adhesives

3. Results and Discussion

Many simulations were performed for the purpose of investigating the effects of camber and vortex generators on the morphing airfoil's aerodynamic performance; that is, 4 cases were done:

i. Uncambered, No VGs
ii. Uncambered, With VGs
iii. Cambered, No VGs
iv. Cambered, With VGs.

For each of the configurations mentioned, crucial parameters like lift-to-drag ratio, boundary layer separation, turbulent kinetic energy and turbulent intensity as the angle of attack was increased were then examined.

3.1 Uncambered, No VGs

The baseline NACA 0009 design in Case 1 demonstrated performance limits as the AOA increased in the absence of camber and VGs; that is, the airfoil had trouble producing more lifts at higher AOAs because it lacked the camber required to improve lift capabilities. The drag caused by lift phenomenon, also known as induced drag, was also highlighted by this constraint; higher induced drag resulted from the lift vector tilting backward as the AOA increased because of downwash produced by wingtip vortices. Moving on, without the implementation of VGs, the airfoil was more likely to experience early boundary layer separation. This separation was particularly visible at AOAs of 16° to 19°, as shown by Figure 11 and Figure 12, when turbulent kinetic energy and intensity increased near the trailing edge, resulting in a rapid induce drag increase. The lack of boundary layer control resulted in a low Cl-Cd ratio due to low Cl and high Cd, restricting the airfoil's ability to generate efficient lift beyond 10° AOA.

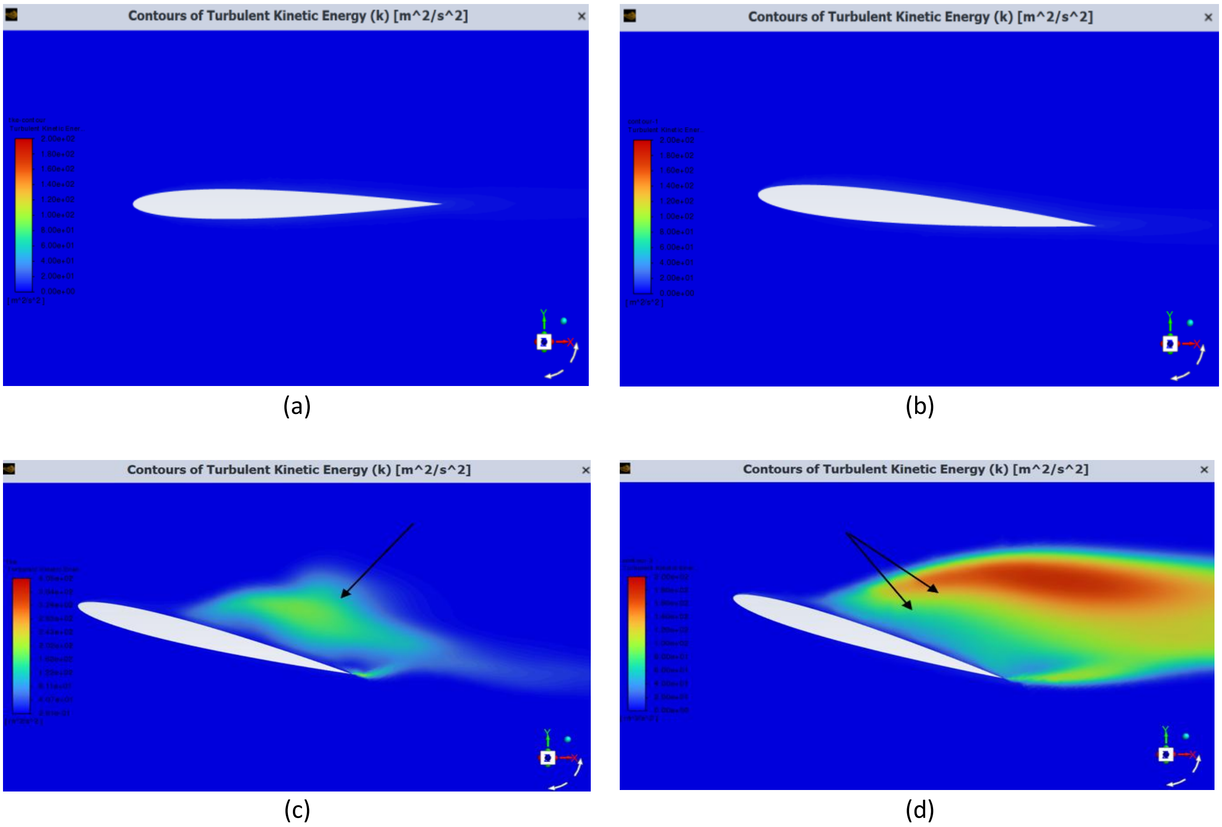

Fig. 11. (a) 0 degrees (b) 10 degrees (c) 15 degrees (d) 18 degrees

Furthermore, in this baseline configuration, the absence of both camber and vortex generators resulted in early boundary layer separation at higher AOA, particularly above 16°. The divided flow formed a wake zone with high turbulence intensity, which increased drag significantly; nonetheless, the principal drag in this case was pressure drag, which was created by a large pressure difference between the airfoil's upstream and downstream sides. Furthermore, at higher AOAs, produced drag from the lift caused by wingtip vortices reduced performance even further. Without camber to smooth the airflow, circulation around the airfoil was restricted, resulting in limited lift generation and a low lift-to-drag ratio.

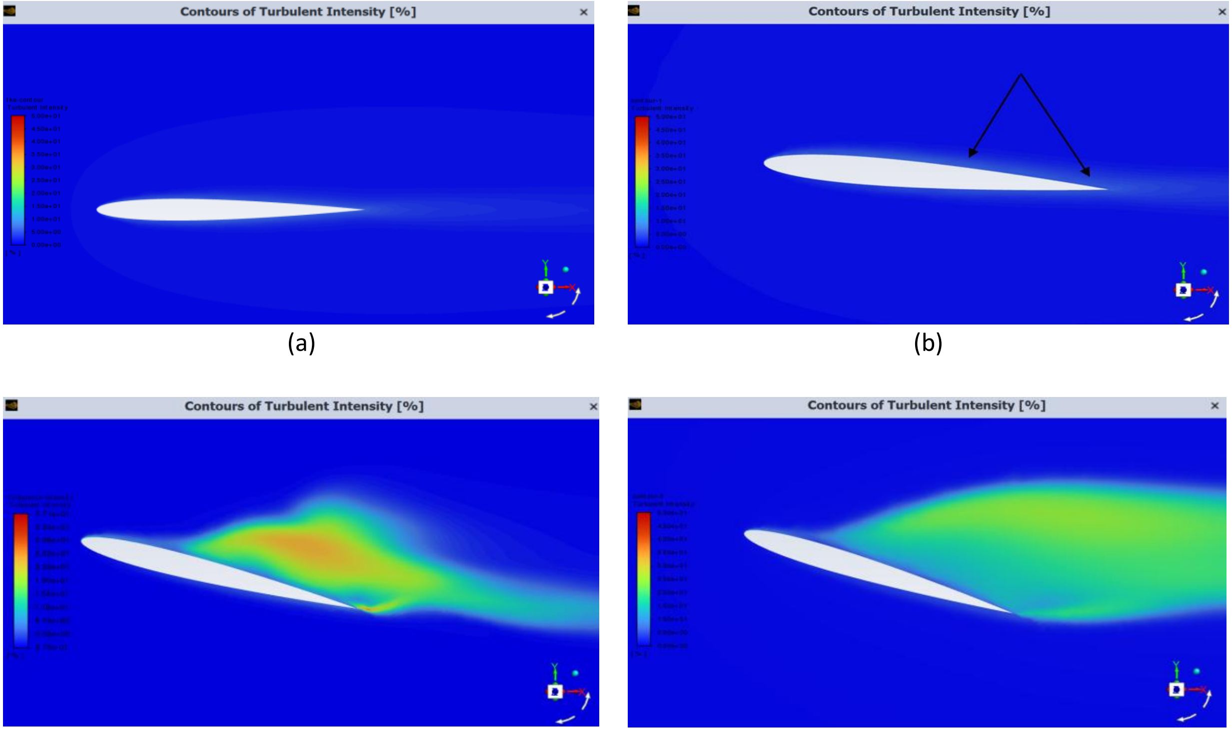

(a) (b) (c) (d)

Fig. 12. (a) 0 degrees (b) 10 degrees (c) 15 degrees (d) 18 degrees

3.2 Uncambered, With VGs

As shown in Figure 13, Case 2, which featured VGs but no camber, outperformed Case 1 in terms of boundary layer control because the VGs energized the flow and slowed flow separation; as a result, the delay in separation reduced both pressure drag and induced drag, managing Cd. While VGs improved flow behaviour in Case 2, the lack of camber limited the airfoil's ability to generate additional lift because circulation around the airfoil was constrained. To explain how circulation affects the generation of lift, it is critical to implement the Kutta-Joukowski theorem, which states that lift is directly proportional to circulation around the airfoil.

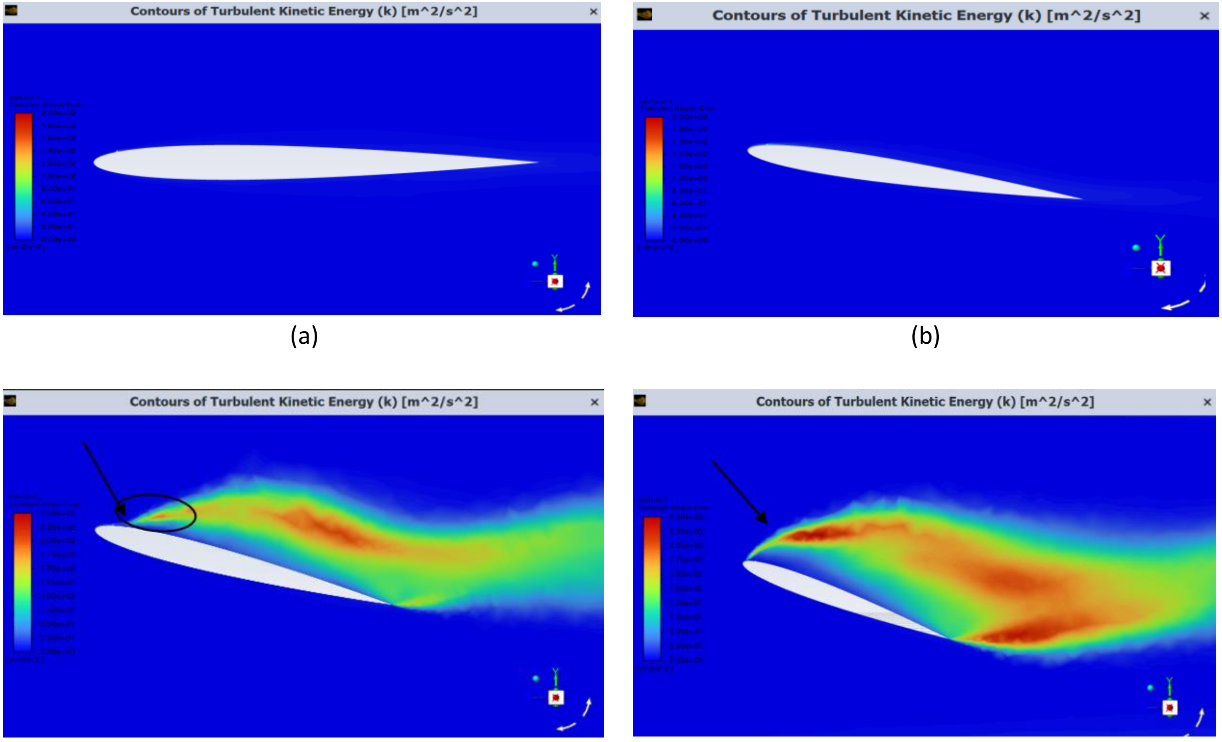

(a) (b) (c) (d)

Fig. 13. (a) 0 degrees (b) 10 degrees (c) 15 degrees (d) 18 degrees

Adding vortex generators to the uncambered airfoil mitigated early flow separation by energizing the boundary layer. Vortex generators introduced streamwise vortices, which enhanced the momentum of low-energy boundary layer flow, delaying separation shown by Figure 14; thereby, this reduced the wake size and turbulent intensity near the trailing edge. Consequently, pressure drag was reduced as the flow remained attached for a longer duration of the airfoil's surface. However, the lack of camber restricted the generation of circulation, which is essential for higher lift according to the Kutta-Joukowski theorem.

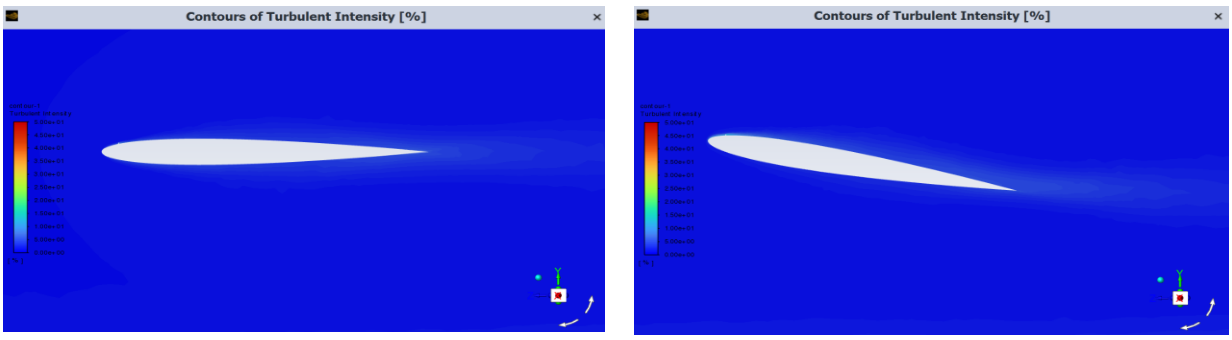

(a) (b)

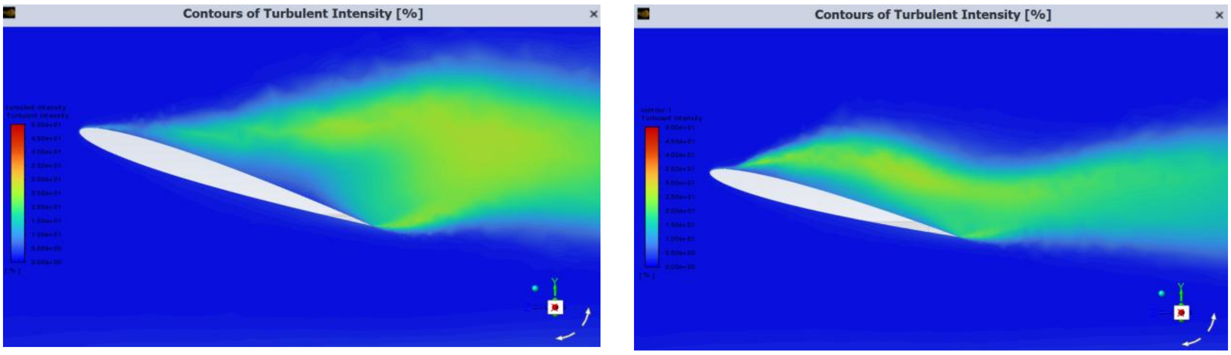

(c) (d)

Fig. 14. (a) 0 degrees (b) 10 degrees (c) 15 degrees (d) 18 degrees

3.3 Cambered, No VGs

In Case 3, demonstrated by Figure 15, which lacked VGs but had camber, the extra camber improved circulation by guiding airflow more effectively over the airfoil and towards the leading edge (Kutta Condition), where the 2nd stagnation point is. This enhanced circulation resulted in more lift generation compared to Cases 1 and 2. However, the lack of VGs in Case 3 made it vulnerable to early boundary layer separation at higher AOAs, beginning at 17°. Thus, this early separation disturbed the smooth airflow required to sustain lift, resulting in a sudden increase in drag from turbulence wake generation near the trailing edge, thus improving Cl-Cd ratio compared to Case 1.

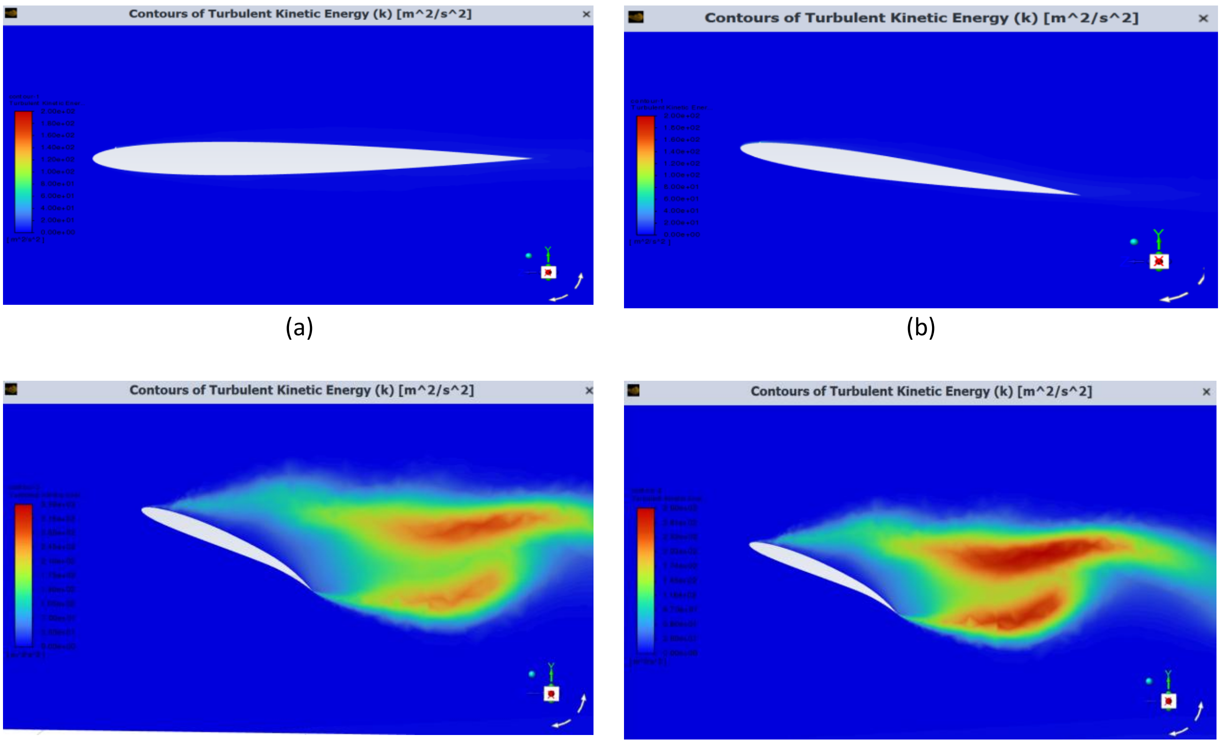

(c) (d)

Fig. 15. (a) 0 degrees (b) 10 degrees (c) 15 degrees (d) 18 degrees

Camber also modified the stagnation points, increasing pressure on the lower surface while decreasing pressure on the top surface. However, the absence of vortex generators exposed the airfoil to adverse pressure gradients, resulting in early boundary layer separation at higher AOAs. Thus, this separation increased turbulence intensity in the wake zone, resulting in higher pressure drag and worse aerodynamic efficiency as shown in Figure 16. The absence of VGs to energize the boundary layer limited the airfoil's ability to maintain attached flow at critical AOAs.

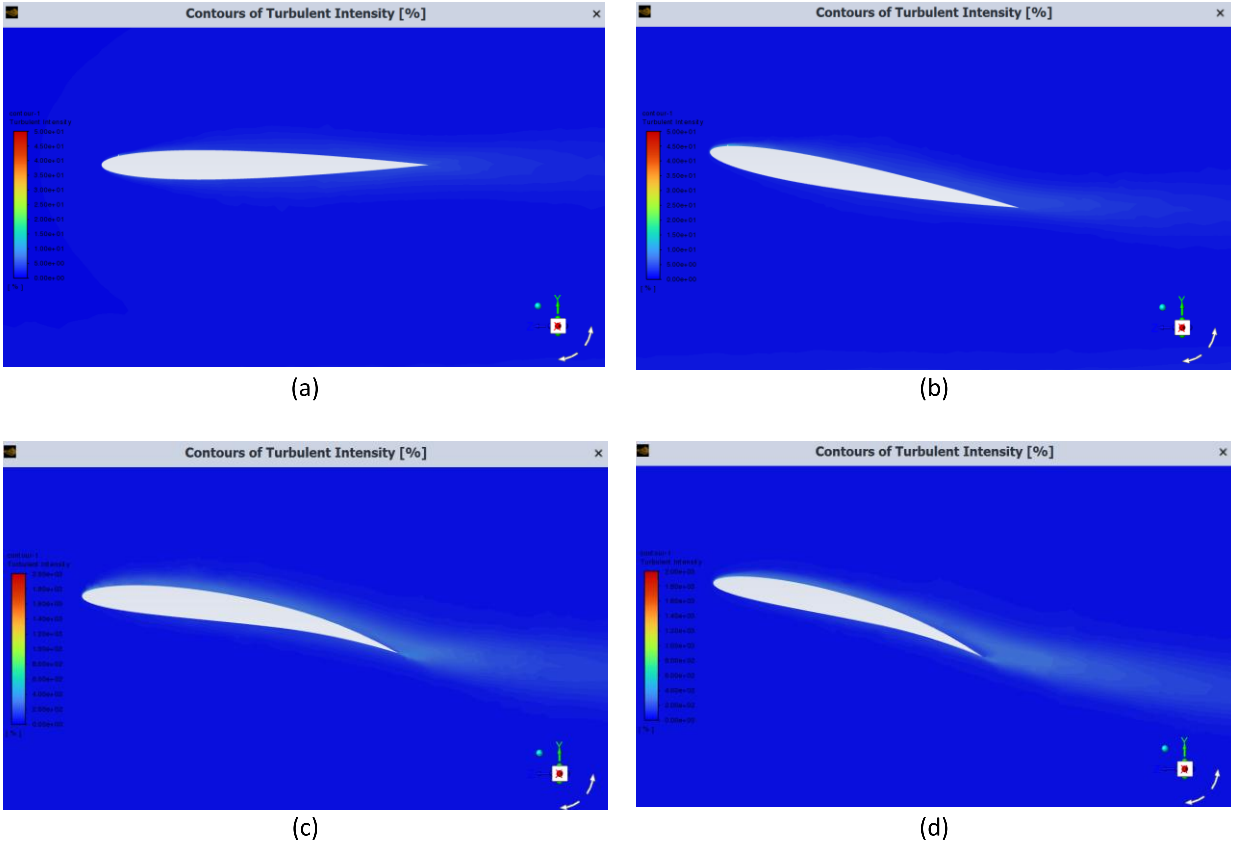

Fig. 16. (a) 0 degrees (b) 10 degrees (c) 15 degrees (d) 18 degrees

As per the table shown above, the variance in speed affected the lift and drag coefficients of the airfoil significantly as per the definition of C_L, where it is inversely proportional to the air velocity; thus, after confirming the drag and lift coefficients from the literature [24] at a similar AoA. Figure 7 and Figure 8 below show drag and lift convergence plots at reference conditions.

3.4 Cambered, With VGs

In Case 4, the combination of camber and VGs produced the greatest simulation results, particularly at high AOA, e.g., around 19°, as shown by Figure 17. The VGs effectively delayed flow separation by energizing the boundary layer, which mitigated the negative impacts of induced drag at higher AOAs, revealed by Figure 17; by preventing early flow separation, the VGs reduced the downwash impact. This enhancement enabled the airfoil to retain efficient lift production without incurring significant drag costs as the AOA increased. Moreover, the cambered design in Case 4 used the Kutta-Joukowski theorem by boosting circulation over the airfoil, resulting in a higher lift coefficient. By adjusting the camber = 4 % and camber position = 70 %, the airfoil created a favourable pressure differential, resulting in greater Cl and minimized Cd at increasing AOAs. The seamless detachment of flow at the trailing edge, enforced by the Kutta condition, helped to manage circulation, allowing Case 4 to maximize lift and minimize drag at high AOAs.

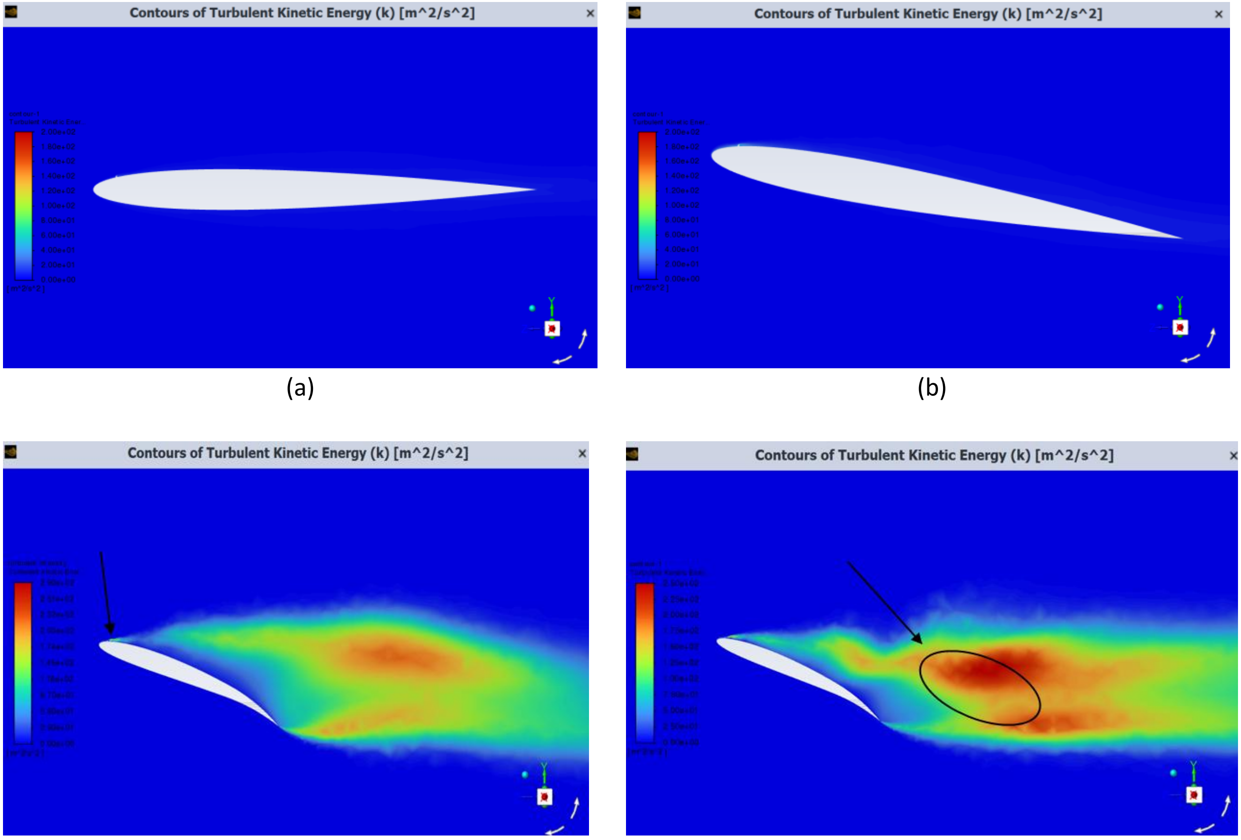

(a) (b) (c) (d)

Fig. 17. (a) 0 degrees (b) 10 degrees (c) 15 degrees (d) 18 degrees

Finally, the camber improved circulation and lift by generating a positive pressure difference between the top and lower surfaces as shown in Figure 18. Meanwhile, vortex generators powered the boundary layer, reducing pressure gradients and delaying flow separation. This reduced turbulence strength in the wake zone, causing less pressure drag. Additionally, the vortex generators reduced downwash effects, resulting in a larger vertical lift vector. The delayed separation enhanced overall boundary layer stability, allowing the airfoil to have higher lift and minimized drag, resulting in greater Cl-Cd ratio.

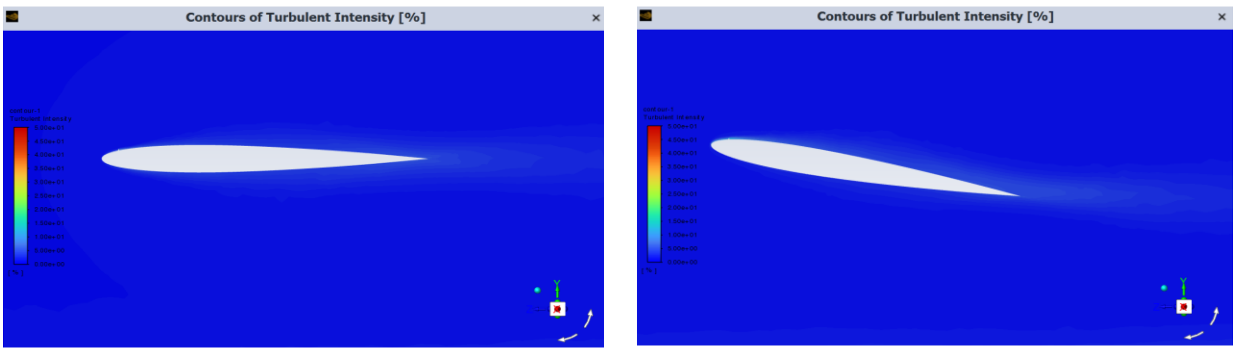

(a) (b)

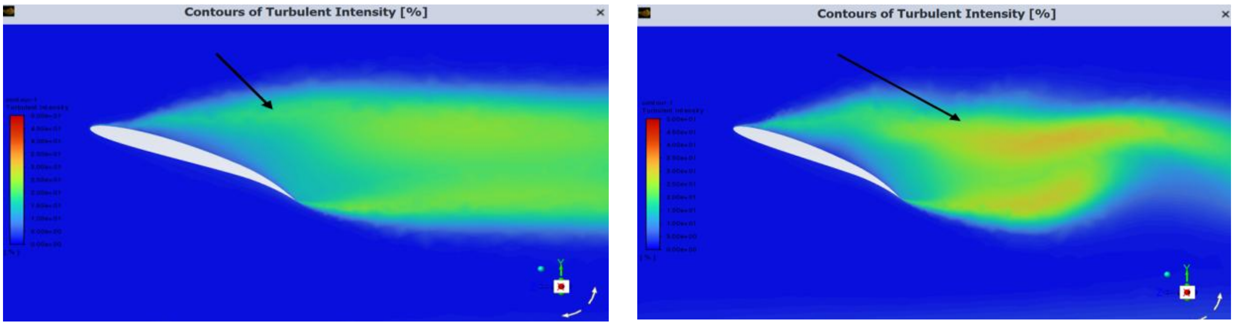

(c) (d)

Fig. 18. (a) 0 degrees (b) 10 degrees (c) 15 degrees (d) 18 degrees

Table 5 summarizes the approximate values acquired from the numerous simulations performed. There are '- 'identified in several cells as the critical angles for these particular cases were reached. In addition, the following paragraphs summarize the findings for each case.

Initially for Case 1, the Cl-Cd ratio quickly dropped as the AOA increased; drag increased dramatically as flow separation occurred at increasing AOAs, stalling at 20°, due to the lack of camber and VGs, which limited lift generation in the absence of boundary layer control. Compared to other cases, this resulted in a relatively low Cl-Cd ratio, indicating poor aerodynamic efficiency. Also compared to work produced by Görgülü *et al.,* [24], the results yielded similar Cl and Cd results at high AOA, roughly 16° to 17°.

For Case 2, across a range of AOAs, the use of VGs increases the boundary layer's adhesion to the airfoil surface even when the AOA increases by stimulating it with small vortices. The stabilizing effect of VGs assisted in controlling the boundary layer, which enhanced lift generation and resulted in a slower growth of drag when compared to Case 1. As a result, it had a higher stalling critical angle of approximately 21°.

Moving on, Case 3 involves the application of camber which improved the initial Cl-Cd ratio in comparison to Cases 1 and 2, as lift output rose, particularly at low to moderate AOAs, 5° to 10°. However, in the absence of VGs to control flow separation, drag dramatically increased at higher AOAs, starting at 20°. This setup highlighted the importance of flow control at greater angles while showcasing the generation of lift due to camber.

Finally, across a broad range of AOAs, Case 4 achieved the highest Cl-Cd ratios and good values of Cl and Cd, as well as highest stalling critical angle of approximately 24°. Even when AOA rose, the combination of camber and VGs improved lift generation while preserving boundary layer stability. As a result, the Cl-Cd ratio decreased more gradually. Thereby, this demonstrated the advantages of combining VGs for flow control with camber configurations for generation of lift, as it was the most aerodynamically efficient.

Table 5
Cl-Cd ratios for all cases

	Case 1	Case 2	Camber = 4%, Camber Pos. = 70%			Camber = 4.5%, Camber Pos. = 80%			Camber = 5%, Camber Pos. = 70%		
AOA (°)	CL/CD Ratio	CL/CD Ratio		Case 3	Case 4		Case 3	Case 4		Case 3	Case 4
0	0	0	AOA	CL/CD Ratio	CL/CD Ratio	AOA	CL/CD Ratio	CL/CD Ratio	AOA	CL/CD Ratio	CL/CD Ratio
5	12.20361105	16.3967268	0	0.67264574	3.257142857	0	0.861423221	2.139303483	0	1.026162791	2
10	7.44137931	8.956020942	5	11.04587156	21.80685358	5	10.34883721	17.8	5	11.09004739	16.16906475
15	5.011246944	6.177993528	10	5.395590143	7.892561983	10	4.674986999	8.270676692	10	3.988311688	7.056603774
17	3.143824027	4.748603352	15	3.49382716	5.475982533	15	3.059118236	4.068322981	15	2.859340659	3.78978979
18	1.748395379	2.241313112	20	1.780177891	2.863728564	20	1.822721598	2.546467818	20	1.816870944	2.209375813
19	1.605327298	2.307555239	22	1.480999888	2.35907173	22	1.060140474	2.047063116	22	1.042786498	1.977333488
20	1.473934426	2.001335336	24	-	2.315886862	24	-	2.007182134	24	-	1.894736842
21	-	1.639834711									

Having said that, 1 key observation was acquired as shown by Figure 19, which was the decrease of Cl-Cd ratio at AOA of 5°across all cases. This can be justified by the change of flow attachment on the surfaces of the airfoil, starting roughly at AOA of 15°. For instance, compared to Cl, the Cd starts to increase at a faster rate; in addition, based on the Kutta-Joukowski theorem, lift is directly proportional to circulation, which peaks at moderate AOAs; however, beyond 5°, adverse pressure gradients along the trailing edge rise, causing the boundary layer to stall and eventually diverge. As a result, this separation increases pressure and viscous drags, decreasing the Cl-Cd ratio.

Furthermore, the surface boundary layer becomes more unstable due to the changes in velocities and the increasing turbulent kinetic energy. Turbulent flow behaviour, which raises drag and slows the rate of lift production, is introduced early. Thereby, the consequences of induced drag become more noticeable at increasing AOAs. As lift rises, stronger wingtip vortices produce more downwash. Thus, VGs are necessary for managing early separation because the boundary layer is less able to tolerate the negative pressure gradient in their absence. In cases with VGs, the boundary layer is more stable, but the Cl-Cd ratio begins to decrease since the drag increase continues to outweigh the lift increases.

In addition, the Q-criterion is a mathematical technique for locating and displaying vortices in a flow field. That is, a region where the rotation of fluid constituents (vorticity) predominates over their deformation is referred to as a vortex [25]. Because it can accurately represent coherent vortex structures, the Q-criterion is crucial to understand complex flow patterns and improve aerodynamic designs [26]. Compared to other approaches like the lambda 2 criterion or vorticity magnitude, the Q-criterion yields more consistent and understandable results, especially in turbulent or unstable flows [26].

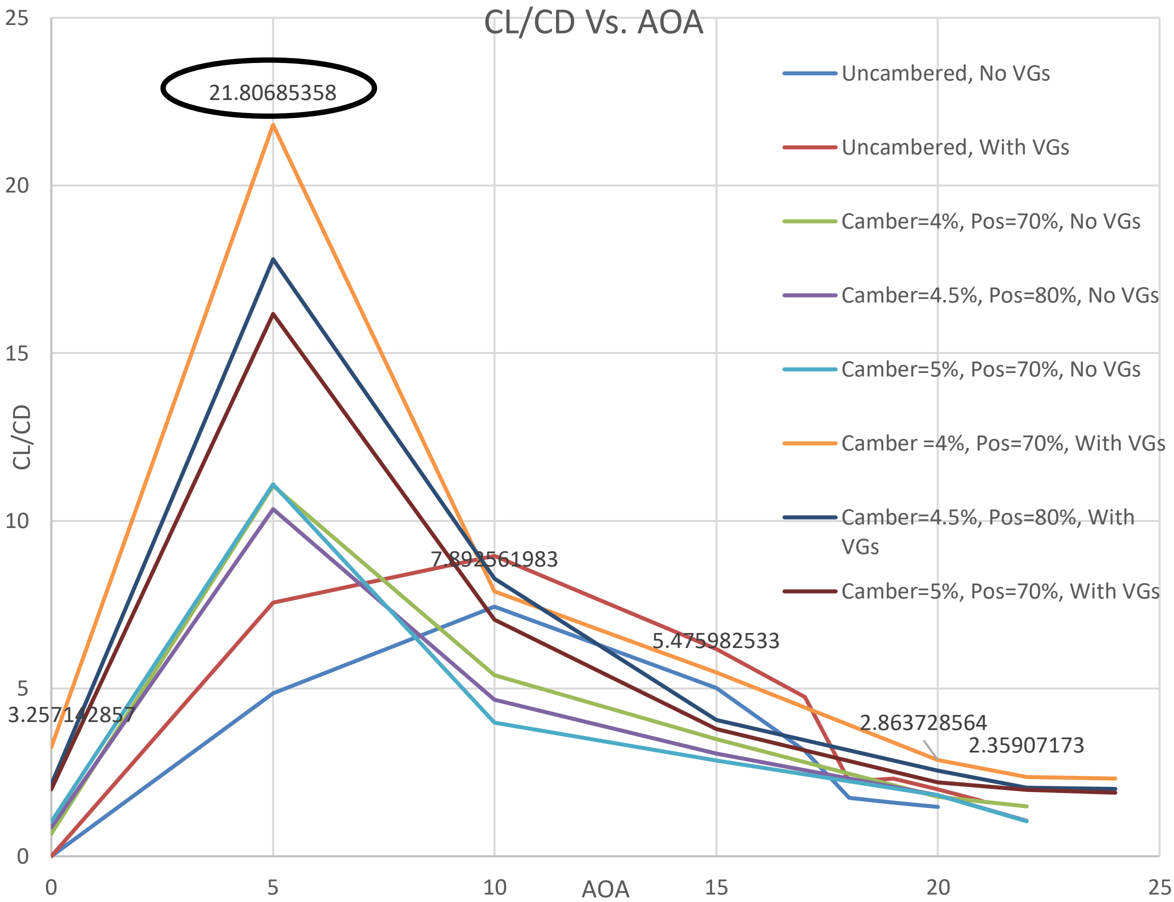

Fig. 19. Cl-Cd ratios for all cases drop at AOA greater than 5 degrees

Furthermore, shown in Figure 20, Case 1 (Uncambered, No VGs) exhibits small vortices at high angles of attack (AOA), especially at the trailing edge [27,28]. Without controlling the boundary layer separation, this implies early flow separation and higher drag. Better vortex control is seen in Case 2 (Uncambered, With VGs) than in Case 1. Smaller, more organized vortices produced by VGs energize the boundary layer and delay separation. In addition, camber causes significant vortex formations at higher AOAs, like in Case 3 (Cambered, No VGs), but it lacks boundary layer stability while increasing lift. Case 4 (Cambered, With VGs) exhibits the best flow characteristics at the end, with small, stable vortices remaining over the surface even at higher AOAs, indicating improved aerodynamic efficiency and controlled flow separation. These differences are shown by the consistent contour scales in each case; Case 4 exhibits the least intense vortex forms, highlighting the necessity of integrating camber and VGs.

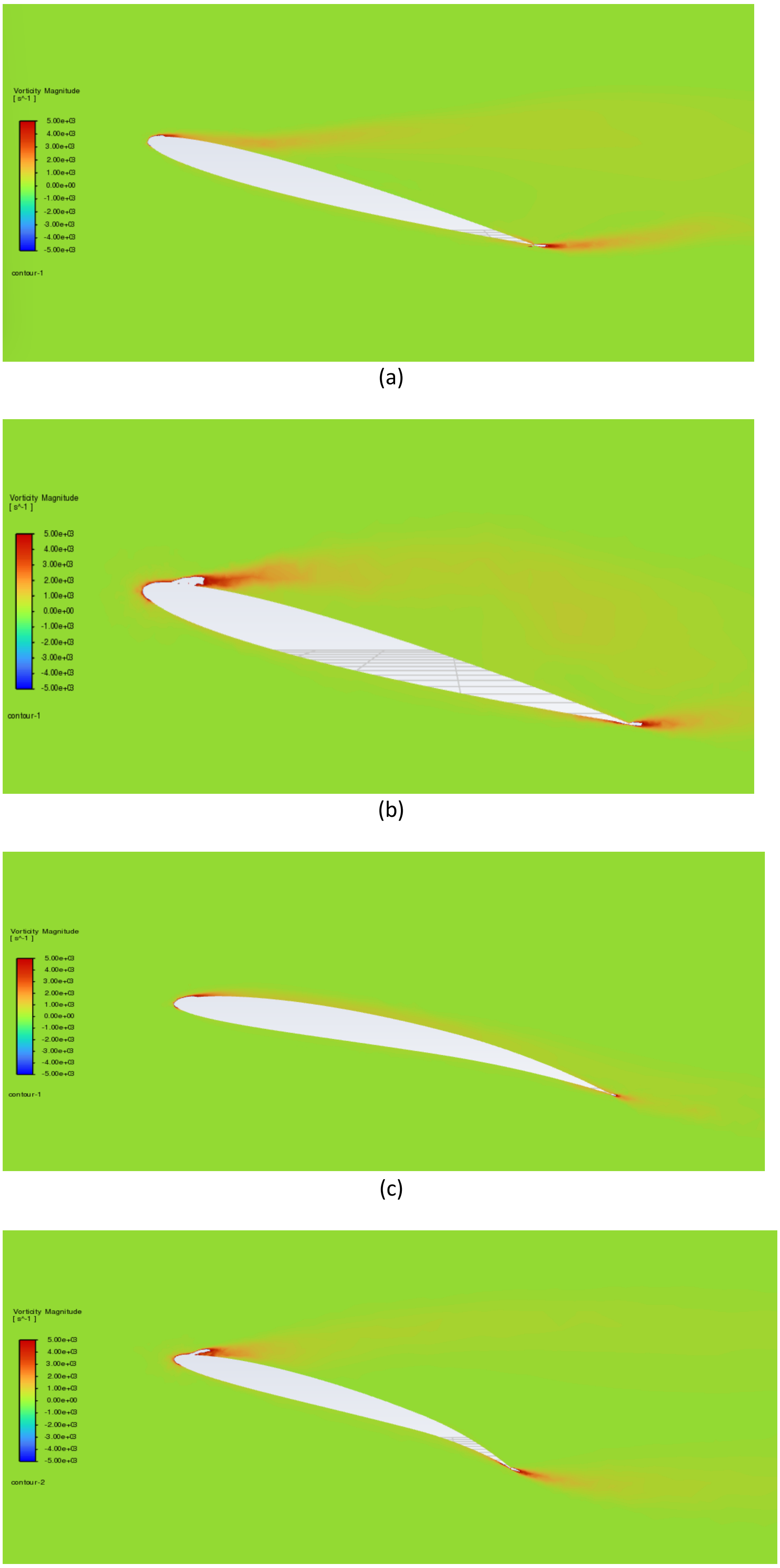

(a)

(b)

(c)

(d)

Fig. 20. (a) Uncambered no VGs (b) Uncambered with VGs (c) Cambered no VGs (d) Cambered with VGs

3.5 Experimental Results

Our experimental results, which show a high degree of accuracy in visualizing flow behaviour across various angles of attack, greatly support the conclusions drawn from our CFD findings; that is, the accuracy of our numerical method is confirmed by the close match between the CFD simulations and the pressure distribution, wake development and flow separation patterns seen in the wind tunnel. For instance, at stalling conditions, the experiment captured the expected large-scale flow separation and unsteady wake turbulence, further reinforcing the accuracy of our CFD-predicted stall characteristics.

Firstly, Figure 21 shows smoke streamlines flowing through the airfoil. At 0 degrees, the airflow remains fully attached on both the upper and lower surfaces. The stagnation point is located at the leading edge, with symmetric pressure distribution on both surfaces. Furthermore, the velocity on the upper surface accelerates, creating a minimal low-pressure region, while the lower surface experiences a slightly higher pressure. The wake is narrow and stable, with minimal turbulence. Most importantly, no significant flow separation occurs and lift is nearly zero due to the symmetric pressure forces. Since there is minimal camber, the pressure difference between the upper and lower surfaces is small, generating low lift but also very low drag.

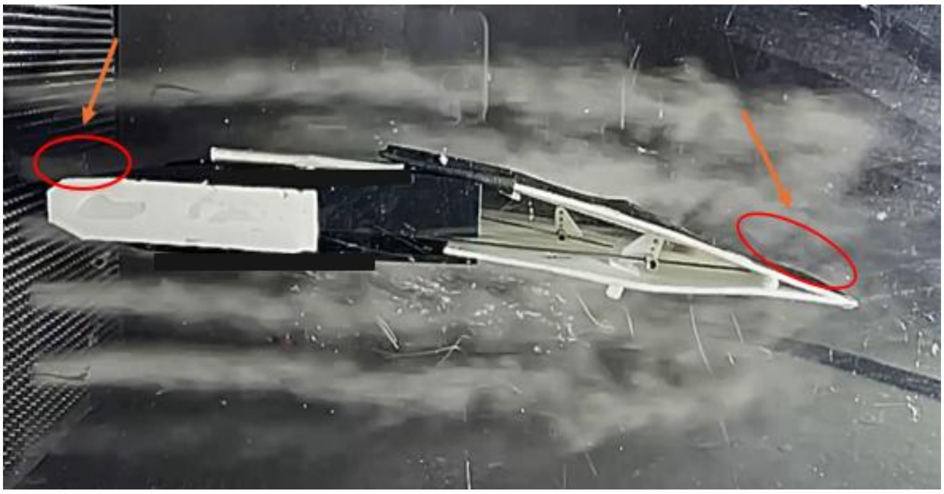

Fig. 21. 0-degree AOA. Streamlines flow smoothly at leading and trailing edges

As the angle of attack increases to 10 degrees shown by Figure 22, the stagnation points shift downward, increasing pressure on the lower surface while the upper surface experiences a stronger suction region due to accelerated flow. The pressure differential between the upper and lower surfaces generates substantial lift. Nonetheless, the wake remains thin and stable, with little separation on either surface. The boundary layer on the upper surface experiences mild adverse pressure gradients but remains fully attached. In addition, the airfoil started to put some camber, but not too significant.

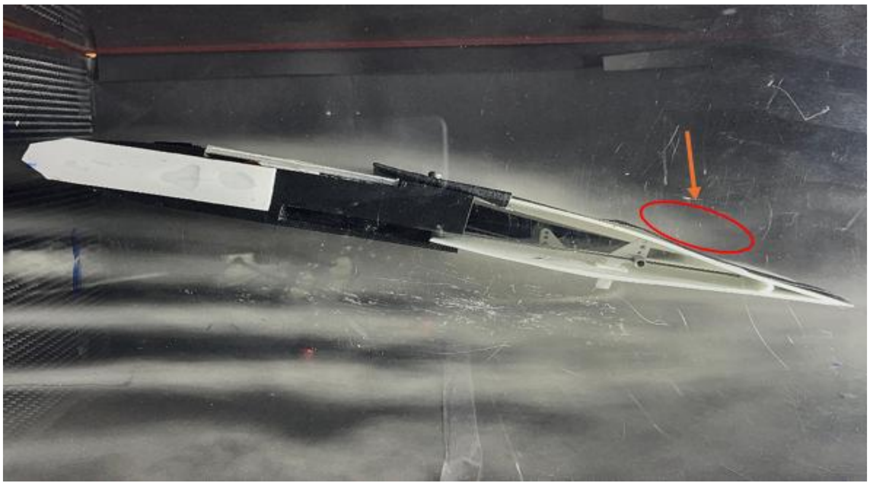

Fig. 22. 10-degree AOA. Minimal flow separation near the trailing edge

As the angle of attack increased to 15 degrees, many observations were made shown by Figure 23. First, the separation point is shifted further up the airfoil's surface. Second, the flow acceleration on the upper surface reaches its peak and the adverse pressure gradient becomes stronger near the trailing edge. Third, the lower surface maintains a high-pressure region, while the wake begins to expand slightly due to increased turbulence. A small separation bubble started forming on the upper trailing edge, signalling the early stall onset. At this angle, lift starts to reach its max generation but drag increases significantly due to greater pressure differences. Wake turbulence begins to increase, though flow on the lower surface remains substantially attached. Having said that, camber morphing reaches a more pronounced curvature, helping to sustain attached flow longer; this allows for an extended suction peak on the upper surface, delaying early boundary layer separation.

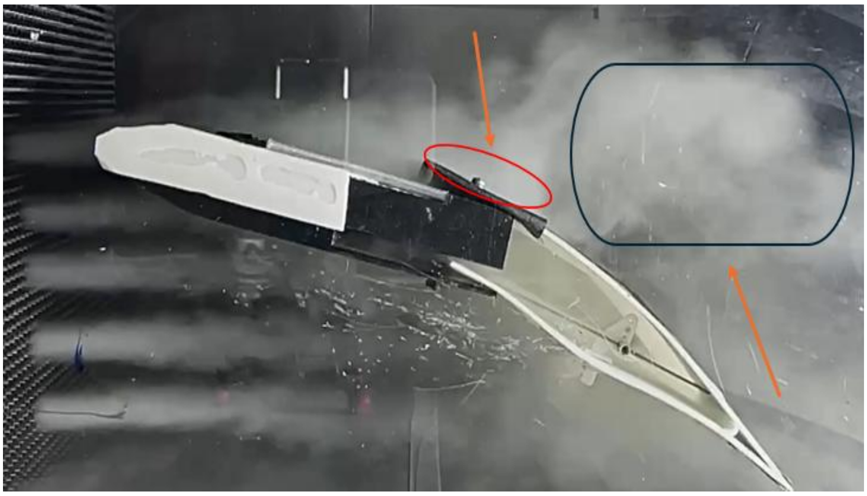

Fig. 23. 15-degree AOA. Flow separation point moved upward the surface, and wake formation begins near the trailing edge

At angle of attack of 18 degrees shown by Figure 24, strong flow separation occurs on the upper surface, creating a large low-momentum recirculating zone. The wake widens significantly and turbulence kinetic energy rises due to strong vortex interactions. Moreover, the flow separation point is moved towards the leading edge and the vortex shedding intensifies, leading to unsteady aerodynamic forces. The camber morphing mechanism allows the lower surface to sustain high pressure, but wake turbulence interacts with the trailing edge, creating pressure fluctuations and unsteady forces. At this point, lift generation begins to decrease and drag increases sharply as the separated flow contributes to a loss in aerodynamic efficiency.

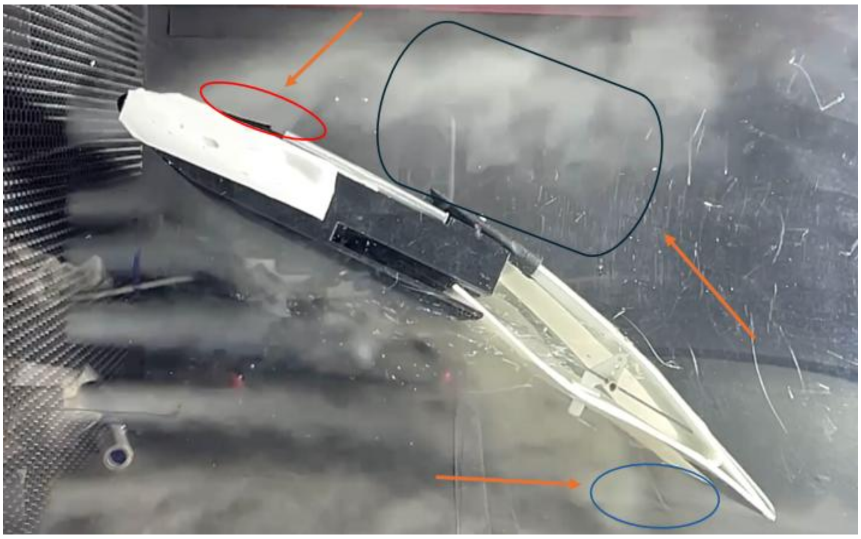

Fig. 24. 18-degree AOA. Flow separation point moved towards near leading edge, wake formation begins near trailing edge

Demonstrated by Figure 25, the airfoil enters full stall at angle of attack of 24 degrees even with the morphing mechanism cannot prevent complete flow separation on the upper surface. The adverse pressure gradient is too strong for the boundary layer to remain attached, leading to a massive loss in lift. Furthermore, wake consists of highly chaotic vortex structures, with strong shear layer instabilities and unsteady flow oscillations. On the other hand, on the lower surface, flow may remain attached in the forward section, but strong pressure fluctuations and local separation near the trailing edge are observed due to wake interaction. Drag is at its maximum and the airfoil could no longer generate substantial lift.

Fig. 25. 24-degree AOA. Flow separation point moved towards leading edge; wake formation increases near trailing edge. Airfoil reaches stall angle

4. Prototype

As shown in Figure 26, the autonomous adaptive wing airfoil's leading part is mechanically designed with PLA+, ensuring a strong and lightweight construction. Furthermore, the airfoil dynamically morphs and adjusts its camber based on Inertial Measurement Unit or IMU, sensor data that detects critical angles in real time. This adaptive feature enables the trailing edge of the airfoil to deflect responsively, improving aerodynamic performance in a range of flight scenarios. Moreover, the servo motors, which are positioned along the airfoil and respond directly to sensor inputs to provide the best possible flight stability and control, allow for exact camber adjustment. This design enables the airfoil to respond to different aerodynamic demands by continuously changing its form in response to changing conditions, providing stability and efficiency.

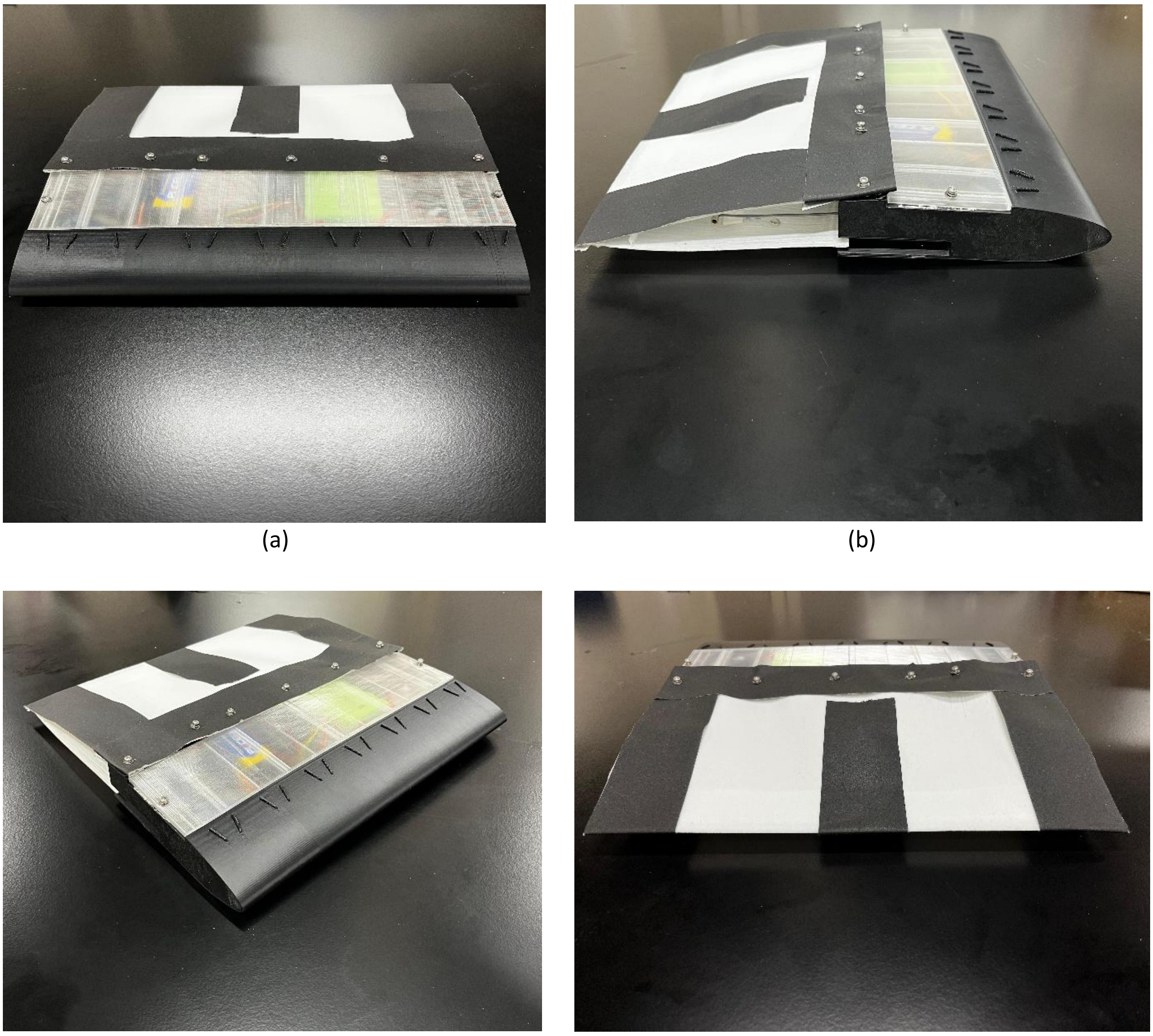

(a) (b) (c) (d)

Fig. 26. (a) Front view (b) Side view (c) Isometric view (d) Back view

Moreover, the servo motor rotated in response to pitch and roll changes detected by the integrated IMU sensor, which caused the trailing part of the airfoil to dynamically change its deflection. When the airfoil hits a critical angle of attack, the system responds by activating the active buzzer, which mimics an aircraft's stall warning indication with a distinctive beeping sound and the Red LED light begins to flash rapidly, signifying danger. The trailing part simultaneously underwent maximal deflection to lower the aerodynamic risk. Once the airfoil stabilizes and reaches safe operating conditions, the servo angles return to their neutral values.

Nonetheless, the most challenging aspect was arranging the wiring and positioning each component in the limited area of the airfoil. Keeping everything compact and neat while ensuring that the cables were securely fastened to the servo motors, sensors and other components was a difficult undertaking. The restricted space made it difficult not only to reduce tangling and interference but also required precise routing to prevent obstructing the airfoil's moving components. Creating a clean, functional layout that maintained reliability and accessibility inside the small facility required a great deal of work and time.

5. Conclusions

This study emphasizes the enormous aerodynamic benefits of adaptive morphing airfoils, with a focus on the combination of camber morphing and vortex generators. A thorough computational examination revealed that the cambered airfoil shape with vortex generators had the best aerodynamic performance of all scenarios studied. The key findings include a significant improvement in lift-to-drag ratio, delayed boundary layer separation and improved stability across a wide range of angles of attack.

The cambered airfoil with vortex generators effectively separated flow by energizing the boundary layer, resulting in reduced pressure drag and increased lift generation. This structure also displayed better flow attachment, especially at higher angles of attack, where standard layouts sometimes induced performance losses. Configurations without camber or vortex generators, on the other hand, showed early flow separation, lower lift and increased drag coefficients, highlighting the relevance of these aspects in performance optimization. Furthermore, the study discovered that integrating vortex generators significantly delayed the start of flow separation, whereas camber improved circulation around the airfoil, resulting in higher lift coefficients. The combination of these properties produced a Cl/Cd ratio that was much higher than that of the baseline design, demonstrating their use in boosting aerodynamic efficiency.

Furthermore, the results of the experiment, which demonstrated a good correlation in wake development, flow separation patterns and pressure distribution, verified our CFD work. Our computational model was confirmed to be accurate when the observed onset of stall and wake turbulence at increasing angles of attack closely matched the numerical simulations.

These findings highlight the potential for morphing airfoil designs to improve aerodynamic performance, especially in applications that require great efficiency and adaptability. Finally, the findings provide a solid platform for developing morphing technologies, proving their capacity to meet fundamental difficulties in modern aerospace design.

Acknowledgement
This research was not funded by any grant.

References
[1] Li, Daochun, Shiwei Zhao andrea Da Ronch, Jinwu Xiang, Jernej Drofelnik, Yongchao Li, Lu Zhang *et al.,* "A review of modelling and analysis of morphing wings." *Progress in Aerospace Sciences* 100 (2018): 46-62. https://doi.org/10.1016/j.paerosci.2018.06.002

[2] Min, Zheng, Vu Khac Kien and Liew JY Richard. "Aircraft morphing wing concepts with radical geometry change." *The IES Journal Part A: Civil & Structural Engineering* 3, no. 3 (2010): 188-195. https://doi.org/10.1080/19373261003607972

[3] Martinez, Joan Marc, Domenico Scopelliti, Cees Bil, Robert Carrese, Pier Marzocca, Enrico Cestino and Giacomo Frulla. "Design, analysis and experimental testing of a morphing wing." In *25th AIAA/AHS Adaptive Structures Conference*, p. 0059. 2017. https://doi.org/10.2514/6.2017-0059

[4] Mugeshwaran, A., Guru Prasad Bacha and S. Rajkumar. "Design and experimental analysis of morphing wing based on biomimicry." *Int. J. Eng. Technol* 7 (2018): 239-244. https://doi.org/10.14419/ijet.v7i2.33.14160

[5] Hussain, S. A. "Review of morphing wing." PhD diss., Phd Thesis, 2017.

[6] ElGhazali, A. F. and Sharul Sham Dol. "Aerodynamic optimization of unmanned aerial vehicle through propeller improvements." *Journal of Applied Fluid Mechanics* 13, no. 3 (2020): 793-803. https://doi.org/10.29252/jafm.13.03.30414

[7] Kaygan, Erdogan, Tugce Koroglu and Melisa Basak. "Aerodynamic efficiency analysis of variable morphing wings." *International Journal of Aeronautics and Astronautics* 3, no. 2 (2022): 71-86. https://doi.org/10.55212/ijaa.1088399

[8] Navrátil, J., V. Hostinský and J. Sodja. "Design of morphing wing for aerodynamic performance considering the wing flexibility effects." In *Journal of Physics: Conference Series*, vol. 2716, no. 1, p. 012029. IOP Publishing, 2024. https://doi.org/10.1088/1742-6596/2716/1/012029

[9] Akhter, Md Zishan, Ahmed Riyadh Ali and Farag Khalifa Omar. "Aerodynamics of a three-dimensional bionic morphing flap." *Sustainable Energy Technologies and Assessments* 52 (2022): 102286. https://doi.org/10.1016/j.seta.2022.102286

[10] Liu, Hao. *Introduction to Flapping Wing Aerodynamics*. Cambridge University Press, 2013.

[11] Majid, Tuba and Bruce W. Jo. "Comparative aerodynamic performance analysis of camber morphing and conventional airfoils." *Applied Sciences* 11, no. 22 (2021): 10663. https://doi.org/10.3390/app112210663

[12] Jawahar, Hasan Kamliya, Qing Ai and Mahdi Azarpeyvand. "Experimental and numerical investigation of aerodynamic performance for airfoils with morphed trailing edges." *Renewable Energy* 127 (2018): 355-367. https://doi.org/10.1016/j.renene.2018.04.066

[13] Molinari, Giulio, Manfred Quack, Vitaly Dmitriev, Manfred Morari, Patrick Jenny and Paolo Ermanni. "Aero-structural optimization of morphing airfoils for adaptive wings." *Journal of Intelligent Material Systems and Structures* 22, no. 10 (2011): 1075-1089. https://doi.org/10.1177/1045389X11414089

[14] Kabir, Arafat, Abdulkareem Sh Mahdi Al-Obaidi and Felicia Wong Yen Myan. "Review and aerodynamic analysis of NACA 2415 morphing wing for variable span and scale morphing concepts using CFD analysis." In *Journal of Physics: Conference Series*, vol. 2523, no. 1, p. 012033. IOP Publishing, 2023. https://doi.org/10.1088/1742-6596/2523/1/012033

[15] Ismail, N. I., A. H. Zulkifli, M. Z. Abdullah, M. Hisyam Basri and Norazharuddin Shah Abdullah. "Optimization of aerodynamic efficiency for twist morphing MAV wing." *Chinese Journal of Aeronautics* 27, no. 3 (2014): 475-487. https://doi.org/10.1016/j.cja.2014.04.017

[16] Parancheerivilakkathil, Muhammed S., Jafar S. Pilakkadan, Mohammadreza AMOOZGAR, Davood ASADI, Yahya ZWEIRI and Michael I. FRISWELL. "A review of control strategies used for morphing aircraft applications." *Chinese Journal of Aeronautics* 37, no. 4 (2024): 436-463. https://doi.org/10.1016/j.cja.2023.12.035

[17] Wang, Sen, Bryce Horn, Findlay McCormick and Sina Ghaemi. "Experimental evaluation of the flow field induced by an active vortex generator." *Experimental Thermal and Fluid Science* 159 (2024): 111280. https://doi.org/10.1016/j.expthermflusci.2024.111280

[18] Jansen, D. P. "Passive flow separation control on an airfoil-flap model." *Deft University* (2012).

[19] Dol, Sh Sham, S. Shahid Pervaiz, M. Uzair, Sh Khalid Bashir and M. Mustafa Elzughbi. "Design of solar-powered endurance glider with vortex generators." *Renewable Energy Research and Applications* 2, no. 1 (2021): 1-8.

[20] Dol, Sh Sh, Abdullah Khamis, Mohanad Tarek Abdallftah, Mohammed Fares and S. Sh Pervaiz. "CFD analysis of vertical axis wind turbine with winglets." *Renewable Energy Research and Applications* 3, no. 1 (2022): 51-59.

[21] Knepper, Angela Marie. "Examination of three candidate technologies for high-lift devices on an aircraft wing." (2005).

[22] Tsipenko, V. G., M. V. Sagaydak and V. I. Shevyakov. "The use of vortex generators to improve the take-off and landing characteristics of transport category aircraft." *Научный вестник Московского государственного технического университета гражданской авиации* 25, no. 4 (2022): 83-95. https://doi.org/10.26467/2079-0619-2022-25-4-83-95

[23] Alawadhi, H. A., A. G. Alex and Y. H. Kim. "CFD analysis of wing trailing edge vortex generator using serrations." In *EPJ Web of Conferences*, vol. 67, p. 02002. EDP Sciences, 2014. https://doi.org/10.1051/epjconf/20146702002

[24] Görgülü, Yasin Furkan, Mustafa Arif Özgür and Ramazan Köse. "CFD analysis of a NACA 0009 aerofoil at a low reynolds number." *Politeknik Dergisi* 24, no. 3 (2021): 1237-1242. https://doi.org/10.2339/politeknik.877391

[25] Zhan, Jie-min, Zhi-ya Chen, Chi-wai Li, Wen-qing Hu and Yu-tian Li. "Vortex identification and evolution of a jet in cross flow based on Rortex." *Engineering Applications of Computational Fluid Mechanics* 14, no. 1 (2020): 1237-1250. https://doi.org/10.1080/19942060.2020.1816496

[26] B. Kaiser and S. Poroseva, "Poster: Q Criterion Isosurface Visualizations of a Zero-Pressure-Gradient Turbulent Boundary Layer," *68th Annual Meeting of the APS Division of Fluid Dynamics*, (2015). https://doi.org/10.1103/APS.DFD.2015.GFM.P0018

[27] Subramaniam, Kamalleswaran and Wan Salim, Wan Saiful-Islam. "A Review of Experimental Approaches forInvestigating the Aerodynamic Performance of Drones and Multicopters," *Journal of Advanced Research in Experimental Fluid Mechanics and Heat Transfer*, (2023): 1-24. https://doi.org/10.37934/arefmht.14.1.124

[28] Oo, Ye Min, Makatar Wae-hayee and Chayut Nuntadusit. "Experimental and numerical study on the effect of teardrop dimple/protrusion spacing on flow structure and heat transfer characteristics." *Journal of Advanced Research in Experimental Fluid Mechanics and Heat Transfer* 2, no. 1 (2020): 17-32.